Adv. Opt. Techn., Vol. 1 (2012), pp. 79–89 • Copyright © 2012 THOSS Media and De Gruyter. DOI 10.1515/aot-2011-0003

Review Article

Tailoring optical and non-optical properties of interference coating materials through the explicit use of small-scale optical inhomogeneities

Olaf Stenzel*, Ulrike Schulz and Norbert Kaiser

Fraunhofer Institute for Applied Optics and Precision Engineering IOF, Albert-Einstein-Str. 7, 07745 Jena, Germany

*Corresponding author
e-mail: olaf.stenzel@iof.fraunhofer.de
Received November 11, 2011; accepted January 11, 2012

Abstract

Although optical coating deposition techniques have been perfected over decades to prepare optically homogeneous dense coatings with smallest surface roughness, nanostructuring of optical coatings has proven as an effective mechanism to further enhance their performance while reducing their thickness in special cases. Therefore, nanostructure effects can be tackled as additional degrees of freedom for coating design, and can even lead to useful property combinations that are inaccessible to 'classical' coatings prepared on the basis of the traditionally available coating materials. Examples include metal island films as building blocks for spectrally selective absorber coatings for color management or solar energy conversion purposes, as well as motheye structures for antireflection coatings and the combined optimization of optical and non-optical coating properties.

Keywords: absorption; antireflection; interference coatings; nanostructures; optical constants.

1. Introduction

Current optical instrumentation becomes more and more complex. To guarantee durability and high optical performance of any optical component, its surfaces have to be overcoated with specially designed thin film stacks to achieve tailored optical properties as well as surface protection [1]. Clearly, any improved or new optical technology may require modified or new optical coating designs, so that optical thin film design is of utmost importance for the whole field of applied optics.

Any design calculation is based on a theory being valid in the framework of certain model assumptions only. A practically deposited coating will not exactly comply with these idealized model assumptions, and therefore its measured performance will be different from what has been calculated at the design stage. It is then desirable to minimize the discrepancies between theoretically predicted and practically achieved performances to a minimum that is acceptable for the underlying application, but still realistic with respect to the underlying physics. To do so, an elaborated characterization procedure is necessary to understand the reasons for any discrepancies between the measured and expected behaviors.

In practice, this may lead to the situation that characterization of a real sample needs to be performed within physical model assumptions beyond those which have been used in design calculations. For example, a coating designed within the frames of a homogeneous layer model may appear macroscopically stoichiometric, but nevertheless suffers local stoichiometry fluctuations. In the case that these stoichiometry fluctuations occur on the nanometer scale, the layer will still appear optically homogeneous, but suffers absorption losses which cannot be explained based on the average layer stoichiometry alone. Hence, one is confronted with some type of accidental nanostructuring that enforces the extension of the optical model when characterizing such a coating. We will shortly discuss such an example in Section 3.1.3.

The understanding of effects of nanostructuring on the optical properties of interference coatings may therefore be necessary for understanding details of measured thin film spectra. By contrast, once these effects are understood, they can be tackled as additional degrees of freedom in coating design, to comply with specifications which cannot be achieved with homogeneous coatings. We will start our discussion of nanostructured coatings with this situation.

At the first step, optical coating design is a purely computational task. One has to find the construction parameters of thin film systems required to fit a customer-defined specification ('reverse search'). If there are multiple solutions to this task, the designer will choose a design most conveniently to produce in practice. At this step, practical considerations such as stability against process parameter fluctuations, thickness monitoring requirements, and costs become important. To find the optimum solution, more and more sophisticated mathematical algorithms have been developed in the past and implemented into commercially available thin film design software [2–5]. In general, the theoretical apparatus behind the calculations is based on the typical assumptions of homogeneity and isotropy of the film materials.

Although general mathematical theorems are proven which guarantee existence and properties of a theoretical solution for broad classes of thin film design problems (theorem on solvability and maximum principle [6]), practical limitations

occur that may prevent a satisfying design from being found even on the computer. Among these limitations are:

- finite allotted maximum thickness of the whole layer stack,
- finite allotted minimum thickness of individual layers,
- finite allotted maximum number of individual layers in the design,
- finite number of available optical materials, and therefore a finite range of accessible refractive indices and absorption features,
- 'given-by nature' absorption and dispersion of the coating materials, and
- side requirements on non-optical properties of the coating.

At least the last three problems can be tackled by means of nanostructured films. In a narrow sense, instead of using traditional 'pure' coating materials with given by nature individual properties, one could attempt to achieve more design flexibility regarding mixtures of two or more optical materials as building substances for each layer. Once the coating should appear optically homogeneous (particularly to avoid scatter losses), any spatial inhomogeneity parameter resulting from the particular morphology of the mixture (cluster size and inter-cluster distances, pore size, structure period) must be well below the wavelength of the light. Thus, for typical ultraviolet/visible (UV/VIS) coatings, this requirement leads us to inhomogeneity parameters on the nanometer or, at least, 'deep' sub-micrometer scale. In the present paper, we will rather restrict ourselves to this situation.

In a broader sense, nanostructuring may be performed on a larger spatial scale to make explicit use of diffraction effects to tailor the optical properties of a surface. Because such effects are beyond the limits of what is called an interference coating in its traditional understanding, they will not be tackled in this paper. A recent review on this subject can be found in [7].

2. Basic concept

Once the characteristic spatial dimensions characterizing the inhomogeneity in composition of a mixture layer are much smaller than the wavelength of the light, the mixture coating appears optically homogeneous. Its optical behavior can be described by an effective dielectric function or a pair of effective optical constants, which appear to be a possibly complicated function of the optical constants of the constituents, their volume fractions, and morphology in the mixture [8, 9]. These effective optical constants can therefore be tailored to a behavior that is not observed in any known pure material, but might be close to what is required in a particular application.

The general practical potential of tailoring optical constants by intermixing two different components is visualized in Figures 1 and 2. In Figure 1, the result of the model calculation of the dielectric function (DF) of a mixture is shown, as obtained in terms of the Maxwell Garnett model [10] (see Appendix 1). Thereby, the host DF was assumed to be real with $\mathrm{Re}\varepsilon_{host}=\varepsilon_{host}=2.25$. The host material is thus purely dielectric. For simplicity, the inclusions are assumed to be spherical and to occupy 20% of the volume of the mixture. While the imaginary part of the inclusions DF is kept fixed

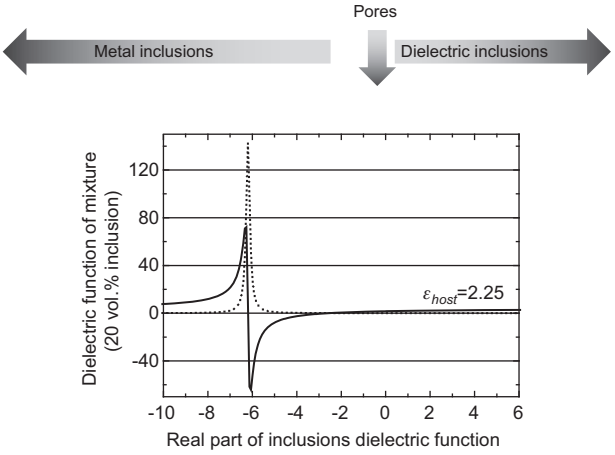

Figure 1 Model calculation: effective dielectric function (full line: real part; dotted line: imaginary part) of a mixture in dependence on the real part of the inclusions dielectric function (Maxwell Garnett model).

with $\mathrm{Im}\varepsilon_{incl}=0.01$ for avoiding singularities, Figure 1 shows the impact of changes in the real part of the inclusions DF on the effective DF of the mixture.

In that somewhat unusual representation, we identify three principal regions of accessible effective dielectric functions:

- In the case of negative real parts of the inclusions DF, Figure 1 reflects the effects caused by nanometer-sized metallic inclusions in a dielectric host, e.g., typical metal island films [10, 11]. Both real and imaginary parts of the mixture DF may vary in wide regions due to the optical excitation of surface plasmons in the metal spheres.
- In the case of an inclusion DF in the range between 1 and 2, the inclusions can be understood as voids in the host which

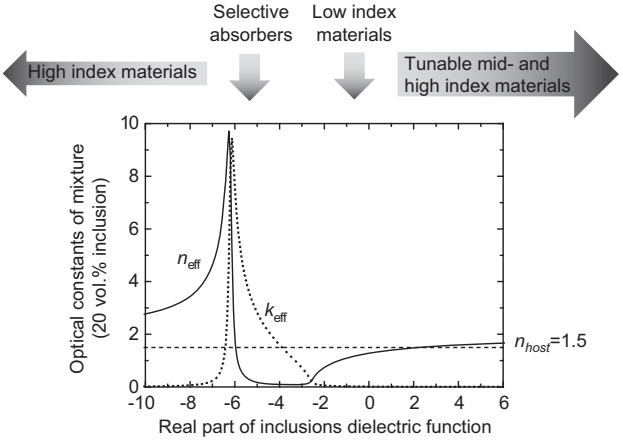

Figure 2 Model calculation: effective optical constants (full line: refractive index; dotted line: extinction coefficient) of a mixture in dependence on the real part of the inclusions dielectric function (Maxwell Garnett model). The dashed line shows the refractive index of the host material.

are empty or (partially) filled with water. This situation is typical for nanoporous dielectric coatings [12, 13].
- When the inclusions DF (real part) is larger than approximately 2, the inclusion can be understood as a dielectric inclusion composed from practically available dielectric coating materials, and what we have is a dielectric mixture with an effective DF tunable by the properties of the inclusions [14].

In the present study, we will not focus on dielectric mixtures. The reader is referred to existing work [14–18] in that regard. Our focus is clearly on the first two regions. When calculating the effective optical constants (refractive index n and extinction coefficient k) from the DF of the mixture via Eq. (1),

$$n+ik=\sqrt{\varepsilon} \tag{1}$$

We immediately see that the metal-dielectric composites can be used as spectrally selective absorbers because of the high effective k-values achievable close to resonance conditions (Figure 2). Nanoporous materials, however, can be used to decrease the refractive index of the mixture with respect to the corresponding host material. Particularly, we can synthesize low effective refractive indices that are not available from pure materials, but are extremely important in antireflection tasks. The mentioned dielectric mixtures allow tuning of optical constants and non-optical properties to novel property combinations that are not available in pure materials.

In the following sections, we will therefore concentrate on three examples. The first example deals with absorption enhancement in optical surfaces by metal island films. The second example describes spectrally and angular broadband antireflection effects caused by so-called motheye structures. And in the third example, emphasis is placed on compromises which can be achieved between optical and non-optical properties of interference coatings when tolerating nanoporosity in the films.

At the end of this section it is worth mentioning that all design and characterization tasks have been performed using conventional thin film calculation software, keeping in mind that the 'normal' optical constants in these calculations are conceptually replaced by the effective optical constants of the mixtures. The dispersion of these effective optical constants can look unfamiliar to optical coating experts (this is particularly valid for metal island films), so that some rather specialized optimization routines may fail to converge, but as it has been shown in different studies, suitable choice of dispersion models or the inclusion of regularization terms into the minimization algorithm turn out to be effective tools to overcome this problem [19–21].

3. Applications

3.1. Metal island films for absorption enhancement

3.1.1. General principle Noble metal island films represent a particular case of nanostructured cluster material [10, 11]. They are built as a (nearly) planar arrangement of individual noble metal particles (which are called islands or clusters) with characteristic sizes usually ranging from a few to a few tens of nanometers. They may effectively absorb light due to the excitation of surface plasmons, and are therefore a natural choice as building blocks for spectrally selective absorbers. During the past decades, a multiplicity of research papers has appeared where different approaches have been developed to relate the optical properties of these island films to the specific size, shape, orientation, arrangement, and environment of the individual islands. It appears as a rather subjective matter to select the most important from them, but there is no doubt that the basic theory has been developed by Gustav Mie [22, 23]. In the quasistatic approximation, when the size of an individual cluster (or island) is much smaller than the wavelength of the light, simpler equations apply for the response of a single island, and particularly effects caused by deviations from a spherical island shape can be described in terms of depolarization factors [24–26]. Yamaguchi et al. also discussed the influence of a non-symmetric dielectric environment of the clusters [27]. In the work of Gerardy and Ausloos [28], a so-called generalized Mie theory was developed with the purpose to calculate absorption and scattering losses of aggregates of spherical clusters [29], taking the electrodynamic interaction between the single clusters into account. Lebedev et al. [30, 31] extended that description to the practically relevant case of an absorbing cluster environment. It is nevertheless common to all these approaches that the optical properties of a metal island film turn out to be extremely sensitive to its geometry, and hence metal island films provide a flexible tool for tailoring the absorptance of an optical surface.

By contrast, it appears troublesome to combine the mentioned theoretical approaches with the standard theory of interference coatings to obtain easy-to-handle design and characterization tools. For practical purposes, an easier approach is possible. Owing to the small size of the metal islands and their small inter-island distances, the description of the optical properties of the island film can be performed within the limits of a homogeneous layer model [19], introducing effective optical constants of the metal island film. Then, these island films become accessible to typical thin film design and characterization software.

In application to selective absorber coatings, the specific advantage of metal island films is in their flexibility of the effective optical constants of the island film, which may be varied by means of different preparation and ambient parameters. This is schematically shown in Figure 3, with a schematic sketch of the effective dielectric function and the optical constants of a silver island film in dependence on the silver coverage, which is expressed in terms of an average silver thickness $<d>$.

The idea of using metal island films in spectrally selective absorber coatings is rather simple. First of all, one has to search for convenient preparation conditions that enable one to produce a metal island film with an absorption behavior that is already close to the required specification. After that, a suitable thin film stack has to be designed which acts

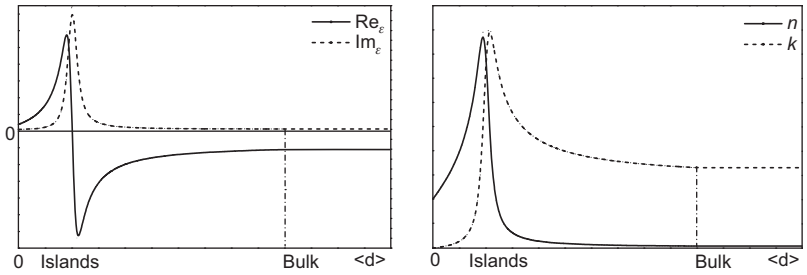

Figure 3 Schematic sketch of the dependence of the effective dielectric function (left) and optical constants (right) of a silver (Island) film on the silver coverage at a fixed VIS wavelength. After the film is closed, the optical constants are no longer dependent on the coverage.

as a resonator for the island film. The goal is to achieve an electric field strength distribution in the stack that couples the light energy effectively into the metal island film only at the required wavelengths. Hence, what we want to do is to combine the intrinsic flexibility in the optical constants of metal island films with the filtering properties of interference coatings. This is visualized in Figure 4.

We deposited several samples of this type while keeping the deposition temperature, but changing the average thickness (as controlled by quartz monitoring) of the silver island film. Figure 5 shows the transmission electron microscopy (TEM) image (in cross-section) of a multilayer sample with a silver island films average thickness of 6 nm. The island film may easily be identified.

Figure 6 shows the main absorption band of the stacks as obtained from measurements of the sample reflectance by A=1-R. As seen from Figure 6, the absorption could be enhanced up to nearly 100%. An increase in the thickness of the silver island film leads to a broadening of the measured absorption structure [32].

Other practical examples of absorber coatings working on this principle have been demonstrated recently [33]. In particular, it has been shown that superior absorption can be achieved in coatings with a smooth gradient in the filling factor of the metal inclusions [34].

One of the most important applications of absorption enhancement caused by metal clusters incorporated into a dielectric or semiconducting environment is offered by the rapidly developing field of plasmonic solar cells [35, 36]. This development started from early efforts pursuing enhancement of photovoltaic conversion efficiencies in organic solar cells [37–39]. Although researchers were able to demonstrate an enhancement in conversion efficiency by plasmon polariton excitation by means of a closed silver film in a prism coupler arrangement [37], in subsequent work the enhancement was already achieved through the incorporation of noble metal island films, i.e., nanostructured coatings with a thickness of only a few nanometers [38, 39]. Hereby, an increase in conversion efficiency of an organic tandem solar cell when incorporating an ultrathin gold island film between the two unit cells has been reported in 1990 [38]. The authors assigned the observation to an effect of the gold island film on the recombination efficiency of the charge carriers [38]. Later on, in 1995, the effect of different types of noble island films on the conversion efficiency of phthalocyanine-based organic solar cells was studied [39]. The authors came to the conclusion that the enhancement in conversion efficiency should be attributed to resonant light absorption in the metal island films, while both plasmonic excitations and interband transitions in the metal are contributing to the effect [39].

Since these pioneering studies, hundreds of research papers have appeared in this field. Current research is reported to be focused on exploitation of electric near field enhancement and effective light trapping caused by optimized plasmonic nanostructures in solar cells [35].

3.1.2. Tuning of the absorption line by means of ultrathin films There are several factors that affect the absorption features caused by metal islands in a dielectric host, such as island size, shape, orientation, as well as inter-island distances. As a matter of fact, the position of the plasmon absorption peak further depends on the dielectric

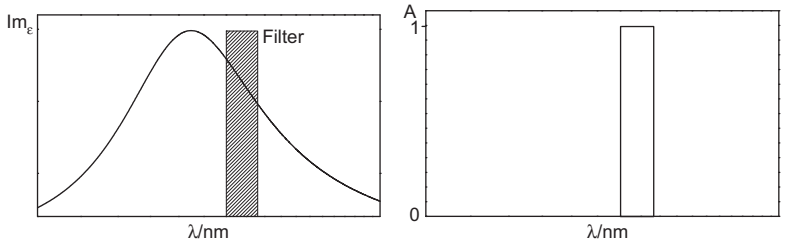

Figure 4 (Left) Imaginary part of the effective dielectric function of a silver island film (line) and comparison with a fictive filter characteristic (hatched). (Right) The dielectric film stack selects only the interesting wavelength region, so that we obtain the required spectrally selective absorption. Owing to constructive interference, the absorptance can be enhanced up to values close to 100%.

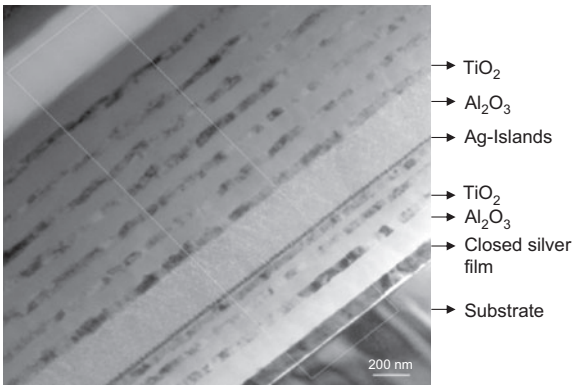

Figure 5 Cross-sectional TEM image of a multilayer sample.

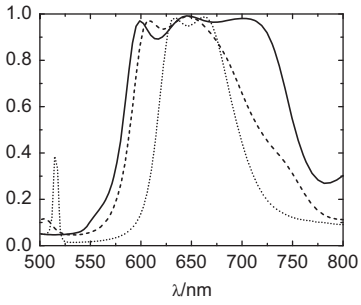

Figure 6 The absorptance of multilayer stacks with a silver island film. The samples differ in the average thickness <*d*> of the island film; dot: 3 nm Ag-islands; dash: 6 nm Ag-islands; solid: 8 nm Ag-islands.

function of both the inclusion and the host material [10]. The rule of thumb is that an increase in the refractive index of the host is accompanied by an increase in the absorption wavelength. Thus, a thin silver island film as deposited on fused silica and kept in air will usually show an absorption maximum in the region between 400 and 450 nm. When embedded in amorphous silicon (a-Si), the absorption peak is located around 700 nm due to the high refractive index of the surrounding medium. Embedding the silver island film into an ultrathin a-Si layer, the absorption frequency of the silver island film can be tuned between these wavelength limits by a suitable choice of the thickness of the (high index) a-Si film [40]. The result of such an experiment is demonstrated in Figures 7 and 8.

Figure 7 shows the TEM image of a silver island film (as prepared by thermal evaporation) in amorphous silicon (as prepared by ion beam sputtering, the silicon thickness is 22 nm). On the top, the silver islands are visualized in a lateral image, they appear as dark spots. On the bottom, we see a cross-sectional image showing the islands arranged in the center of the ultrathin silicon film. In that case, the silver film has maximum absorption around a wavelength of 700 nm.

Figure 8 demonstrates the dependence of the measured peak absorption wavelength of silver and indium clusters on

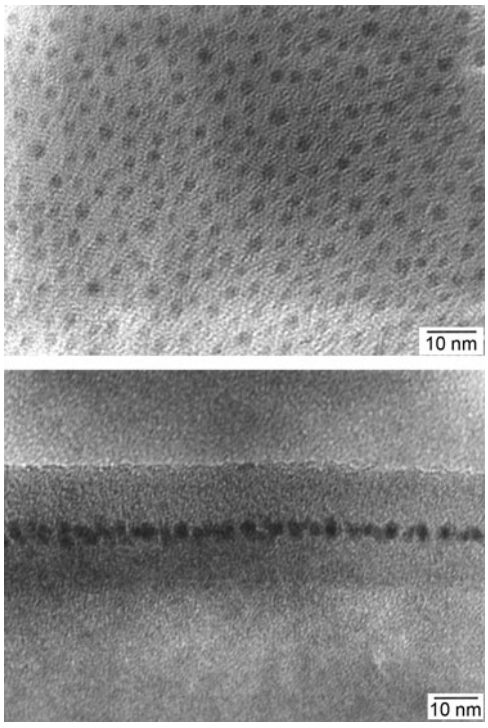

Figure 7 Silver islands embedded in an amorphous silicon film [40]. (Top) Lateral image, (bottom): cross-sectional image.

the thickness of a surrounding a-Si film. The impressive result is that the plasmon absorption wavelength can be tuned over the full visible spectrum by changes in the a-Si thickness for only 10 nm. The large sensitivity in the optical properties to geometrical parameters which are changed on the nanometer scale is one of the most striking features of nanostructured coatings. Practically, it allows us to perform large changes in optical coating properties with a minimum in film thickness. This effect can be assigned to the high electric field concentration as observed in the optical near field region of excited metal clusters [10]. Further relevant practical studies based on the same principle have been published elsewhere [41, 42].

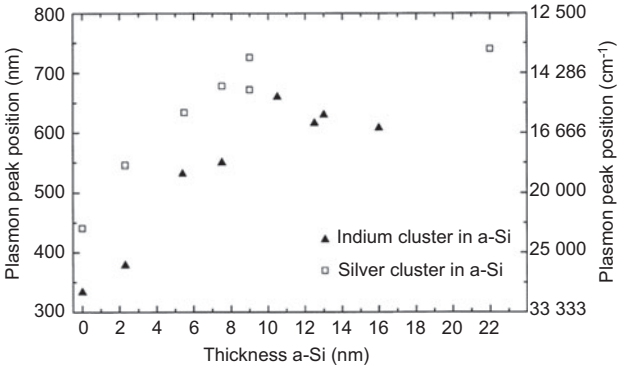

Figure 8 Measured peak absorption wavelength of silver and indium islands in dependence on the thickness of an embedding ultrathin a-Si film [40].

3.1.3. Application to a thin film characterization task: locally understoichiometric fluoride coatings As mentioned in Section 1, fluctuations in the layer stoichiometry may lead to significant absorption losses in coatings which are expected to be rather transparent when taking the average stoichiometry into account only. An extreme example is provided by fluoride layers deposited by a plasma ion assisted electron beam evaporation technique (PIAD) [9, 43]. Well stoichiometric lanthanum or magnesium fluoride layers are transparent down to deep ultraviolet wavelength values. When deposited by traditional evaporation, those layers are, however, porous, which may be disturbing in high-end applications. Therefore, significant effort has been applied to depositing dense fluoride coatings by different ion or plasma assisted deposition techniques [44–50].

Concerning the mentioned PIAD technique, as-deposited fluoride layers show rather strong absorption losses, which can be reduced after deposition by a suitable post-treatment, exposing the layers to UV irradiation [9]. After having tested different physical mechanisms with respect to their ability to explain the measured absorption in a quantitative manner, a consistent mechanism could be identified regarding the absorption losses as being caused by locally occurring understoichiometric areas in the fluoride coating. The mechanism itself has been modeled in a quantitative manner, theoretically replacing the 'understoichiometric' areas by small metal spheres embedded into a rather stoichiometric fluoride environment, e.g., locally understoichiometric magnesium fluoride has been modeled by nanometer size magnesium islands distributed in a stoichiometric magnesium fluoride matrix. This way the measured absorption losses could be reproduced in terms of the Maxwell Garnett model (see Appendix 1) assuming volume filling factors around 0.5%, which seems reasonable when taking the average stoichiometry of the layer into account.

3.2. Motheye structures as low effective index films for antireflection purposes

Motheye structures represent themselves subwavelength relief profiles at the interface between two materials. Early reports on motheye structures deal with periodic profiles [51]. More recent investigations have shown that stochastic motheye structures on polymer surfaces can be prepared by a plasma etching process in high vacuum [52].

For calculating the effect of a motheye structure on optical sample properties, the simplest way is to regard the structure as a mixture of bulk film material and the ambient with a depth-depending mixing ratio. Therefore, the motheye structure can be tackled as a thin graded index film with a thickness corresponding to the surface profile depth, and with refractive indices in-between those of the film and the ambient. With a suitable profile depth, a motheye structure therefore provides an efficient antireflection effect at the mentioned interface. Applications address optical surfaces protected against the environment and concern any type of transmissive optics, as well as absorber optimization, again, for example, in photovoltaics.

In Figure 9, a scanning electron microscope (SEM) image of a stochastic motheye structure on a plastic surface is shown. The profile depth, and consequently the effective film thickness, does not exceed approximately 300 nm. Figure 10 demonstrates the mentioned antireflection effect for a both-side treated poly methyl methacrylate (PMMA) sheet. Without the motheye structure, the normal incidence transmittance would be around 92%, and correspondingly lower at oblique incidence.

Novel approaches to broadband antireflection coatings promise superior performance by combining classical antireflection coating designs (see, for e.g., [53]) with a motheye structure prepared on top of the coating [54].

3.3. Porous high-refractive index layers with an optimal balance between required optical and mechanical properties

In the previous section, we made use of a rather strong porosity to generate materials with a rather low effective refractive index. In this section, we will demonstrate that a certain porosity will also be helpful to optimize the properties of high-index layers. This rather astonishing result is obtained when the full complex of optical and mechanical properties is to be optimized in terms of a practically reasonable compromise.

In modern ion and plasma ion assisted versions of optical coating deposition techniques, the high densification of the films as achieved as a result of energetic particle bombardment during film growth leads to film refractive indices close to or higher than reported bulk values [55]. Hereby, the ion plating techniques and reactively pulsed magnetron sputtering are reported to deliver coatings with the highest refractive indices currently known [56]. As an additional advantage of densification, the pore fraction is negligible, so that thermal shift contributions due to penetration of atmospheric water into pores are absent, and hence these dense coatings exhibit thermally stable high-refractive indices. The disadvantage is that the densification results in high compressive stress of the coatings, which may be disturbing in high-end applications and therefore requires special post-deposition treatments to

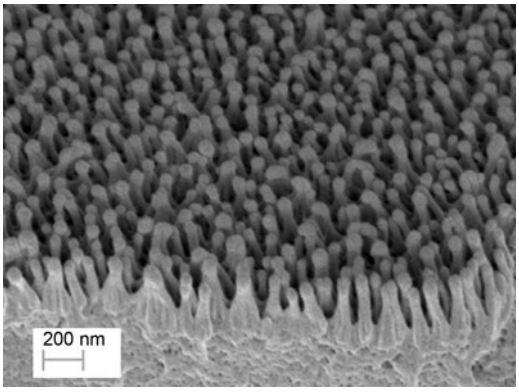

Figure 9 SEM image of a stochastic motheye structure prepared by plasma etching of a PMMA surface.

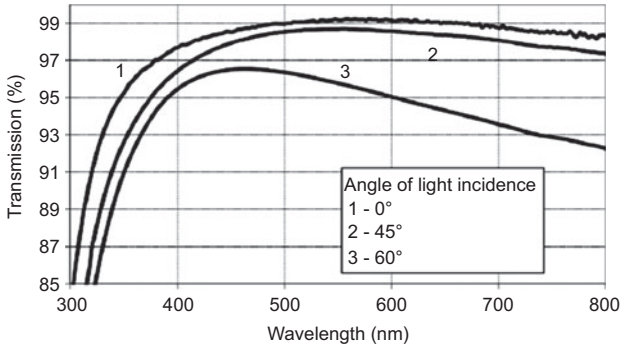

Figure 10 Measured transmittance of a PMMA sheet with moth-eye structures designed for maximum antireflection effect in the VIS on both sides, at different angles of incidence [52]. Polarization is average.

relax the layer stress. Not applying ion assistance during layer deposition usually results in porous layers with significantly lower stress, but at the same time the effective refractive index is also lower and is changing with temperature (thermal shift) due to water exchange with the atmosphere.

In the past years extensive research work focused on the impact of nanoporosity in optical coatings on the interplay between refractive index, thermal shift, and mechanical stress [12, 13]. As a main result it turned out that a small fraction of nanopores in the layer may be beneficial for a practically accepted compromise between these material characteristics. When high-index coatings with negligible shift and negligible stress are required, a key point is that the pores should be small and closed to prevent correspondence (and consequently water exchange) with the ambient medium. TEM investigations really confirmed the existence of small closed pores in nearly stress-free and weakly shifting oxide coatings (see Figure 11).

The mentioned porosity of the films must have an impact on their refractive index, shift and mechanical stress in a well-correlated manner [13]. A relationship between these parameters is shown in Figure 12 for the particular case of tantalum pentoxide layers.

In Figure 12 we recognize simulated as well as experimental points, which correspond to negligible shift, weak stress, and still acceptably high-refractive indices. This property combination corresponds to a practically reasonable balance between optical and mechanical properties. According to the underlying model, these layers should show certain porosity, and the TEM image (Figure 11) of the sample marked by an arrow in Figure 12 (right) really confirms the porosity of the layer. Thus, the main conclusion is that a certain pore fraction (which means an inhomogeneity on the nanometer scale) in these layers is extremely useful for establishing a proper balance between optical and mechanical film properties. For this property combination, pores should occupy only a low volume fraction of the film to keep the refractive index high, they should be closed to prohibit thermal or vacuum shift, and they should be small with a low pore radius for efficient stress relaxation. Practically, this

Figure 11 TEM cross-sectional image of a tantalum pentoxide sample. The pores can be well identified as small bright spots, nevertheless the sample does not show any shift.

means a weak 'nanoporosity' with pore diameters in the range of 1–2 nm is favorable for achieving balanced layer properties.

The theoretical relation between refractive index, shift, and mechanical stress is rather universal and is also observed in other oxide materials. This is demonstrated in Figures 13 and 14. In Figure 13 (left), the typical relation between shift and stress according to the theory (Figure 12, left) is presented. On the right we have experimental hafnia data collected from different sources [12, 57, 58] compared to the relevant theoretical dependence. Finally, Figure 14 demonstrates experimental data corresponding to different oxides coatings and mixtures thereof [14]. In the latter graphs, we recognize that the experimental data are arranged close to a knee-like structure that is theoretically predicted in Figure 13 (left). In particular, we identify experimental points corresponding to the prospective combination of weak mechanical stress and negligible shift, i.e., what we call coatings with balanced properties.

4. Discussion and conclusions

As mentioned at the beginning of this paper, the traditional interference coating theory and technology are entirely based on model assumptions such as ideal homogeneity of the individual coating materials. This requirement is naturally fulfilled in the case where thin film manufacturers prepare rather dense (that means free of pores) coatings composed from pure dielectric materials. The interference coating technology has been perfected in the past decades to comply with that trend. Currently, almost dense coatings are commercially produced by sputtering techniques such as ion beam sputtering, magnetron sputtering, as well as ion or plasma ion assisted

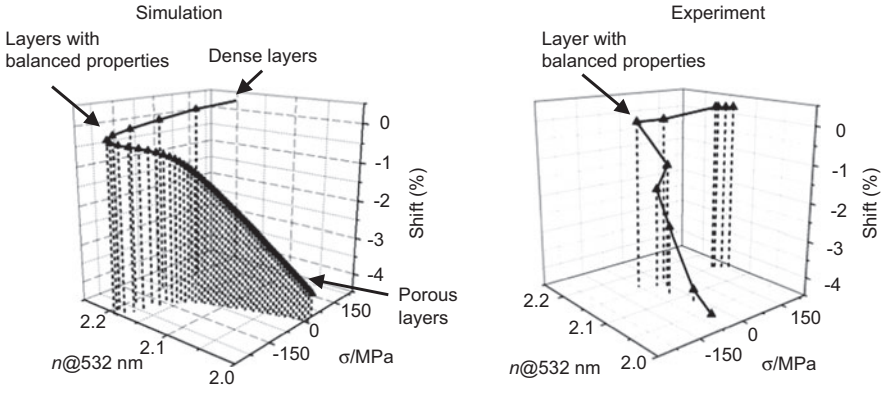

Figure 12 (Left) Simulated [13] correlation between refractive index n, shift and stress σ for the special case of tantalum pentoxide. (Right) Experimental data [13] for tantalum pentoxide layers (prepared by a PIAD technique). The straight connection lines between experimental points serve only as eye guidelines. The arrow indicates the sample from Figure 11.

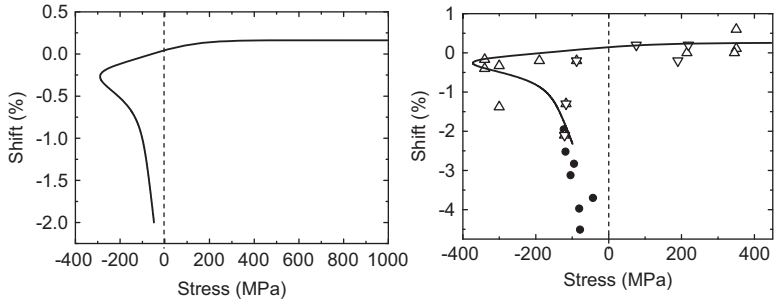

Figure 13 Shift vs. stress. (Left) Theory (corresponding here to Ta_2O_5, see Figure 12). (Right) Full line: theoretical dependence for HfO_2 layers; symbols: experimental data for HfO_2 layers (•: ref. [57], Δ: ref [58], ∇: ref. [12]). Positive stress values correspond to compressive stress. The vertical dashed line corresponds to zero stress.

evaporation techniques such as the already mentioned PIAD deposition method.

By contrast, coating materials that appear inhomogeneous on a nanometer scale are still homogeneous with respect to the interaction with near infra red (NIR)/VIS/UV light, although practical tailoring and controlling of their properties by the preparation process raises new challenges. A practical benefit of nanostructured coatings is the possibility to synthesize materials with effective optical constants not available from nature-given pure materials. It was our intention to provide several examples which should highlight this principal benefit with respect to modern practically relevant technological requirements. We emphasize that all practical examples have been prepared with commercial film deposition coating deposition equipment, so that the preparation of the mentioned nanostructured coatings is fully compatible with interference coating deposition technology.

It was our intention to provide examples on the use of nanostructured optical coatings in very different application fields. Hence, the surface plasmon excitation in metal island films as discussed in Section 3.1 can be utilized for the design of spectrally selective absorbers, for instance, in solar energy conversion applications. In more recent publications, it has been shown that noble metal island films are an effective tool for the color management of optical surfaces [59, 60].

The second group of examples concerned antireflection coating design by synthesizing low-refractive index materials, which led us to the so-called motheye structures.

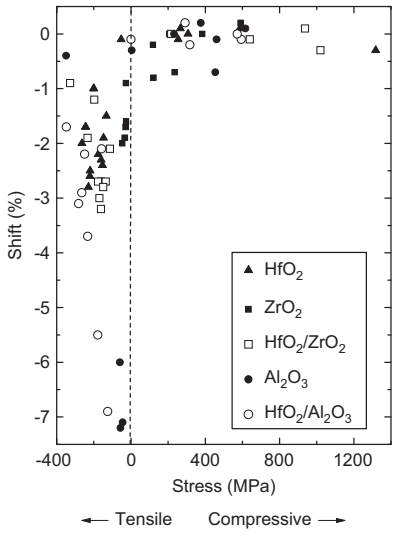

Figure 14 Shift vs. stress for some oxide coatings and their mixtures [14]. The vertical dashed line corresponds to zero stress.

In Section 3.3, we demonstrated an approach for diminishing shift and mechanical stress of high-index coatings by means of nanoporous layers. In fact, these examples principally concern all of the practically relevant thin film specifications [2, 3], because a maximum refractive index contrast between the high- and low-index materials used in the design is favorable for achieving an optimal design solution in most applications [6].

Particularly with respect to narrowline reflector designs, we mention the so-called grating waveguide structures as a further example of a sub-micrometer structured high-index optical coating with promising reflection performance [61]. Owing to their low thickness [62], these structured waveguides can combine high reflectivity with a low surface strain even when the coating material exhibits some mechanical stress. Moreover, the thermal shift in refractive index of the waveguide material can be used for active tuning of the rejection wavelength [63].

In conclusion, we would like to state that the utilization of nanostructure effects in optical interference coating practice is still at the beginning. This might be in contrast to other branches of applied optics such as integrated optics or plasmonics. A reason might be that both theory and technology of optical interference coatings have been established and perfected over many decades to a level that most of the practical requirements concerning the optical performance alone can still be satisfied by classical designs. In crucial cases, the practically biggest challenges are in meeting additional requirements on 'non-optical properties' of the coatings. For that reason, in this paper we also addressed non-optical properties such as mechanical stress. Metal island films, motheye structures or even grating waveguide structures demonstrate that suitably nanostructured coatings can fit a required optical performance with a coating thickness which is significantly smaller than that of comparable by performance classical interference coatings. Consequently, such nanostructured coatings can be less strained and lower in mass, which might be essential for coating components in micro-opto-electro-mechanical systems (MOEMS).

All in all, we strongly suggest that the flexibility of nanostructured coatings in meeting both optical and non-optical coating requirements will be of major importance in optical coatings future.

Acknowledgments

The studies of metallic structures have been sponsored by the TMWFK, Thüringen, under the 'NOB' grant. The authors are also grateful to the Europäische Forschungsgesellschaft Dünne Schichten e.V. (EFDS) and to the Arbeitsgemeinschaft industrieller Forschungsvereinigungen 'Otto von Guericke' e.V. (AiF) for financial support concerning the investigation of the properties of nanoporous oxide coatings. Mixture layers have been investigated in the frames of the TAILOR grant, fluoride layers in terms of the FLUX grant, and oxide layers in terms of the PluTO grant. The authors are grateful to the BMWi and the BMBF, Germany, for financial support in terms of the mentioned grants. In addition, the authors express their thanks to the SPIE (Society of Photooptical Instrument Engineering) for an invited talk at the Conference 'Nanostructured Thin Films IV', which gave us the idea and formed the basis to this extended article [64].

Appendix 1

The Maxwell Garnett model in application to thin film characterization

The Maxwell Garnett, Bruggeman and Lorentz-Lorenz mixing models can all be derived from the assumption that the mixing partners are tackled as inclusions numbered by the subscript j, embedded in a certain host medium [A1]. This assumption leads to the general mixing formula [A1, A2]:

$$\frac{\varepsilon-\varepsilon_h}{\varepsilon_h+(\varepsilon-\varepsilon_h)L}=\sum_j p_j\frac{\varepsilon_j-\varepsilon_h}{\varepsilon_h+(\varepsilon_j-\varepsilon_h)L} \tag{A1}$$

Eq. (A1) defines a relation between the effective dielectric function of the mixture ε, the dielectric functions of the constituents of the mixture ε_j, their corresponding volume filling factors p_j, a host dielectric function ε_h, and a depolarization factor L which depends on the shape of the mentioned inclusions [A3, A4].

In the Maxwell Garnett model, it is further assumed that the mixing partners form a guest-host system, i.e., the morphology of the mixture allows classifying one of the mixing partner as the host material (say the lth one), and the remaining as the guest fractions. Then instead of Eq. (A1), we have:

$$\frac{\varepsilon-\varepsilon_l}{\varepsilon_l+(\varepsilon-\varepsilon_l)L}=\sum_{j\neq l} p_j\frac{\varepsilon_j-\varepsilon_l}{\varepsilon_l+(\varepsilon_j-\varepsilon_l)L} \tag{A2}$$

In the special cases shown in Figures 7, 9 and 11, only two mixing partners can be identified. Thus, in Figure 7, we have (nearly spherical) silver inclusions in a host formed from amorphous silicon; in Figure 9, nearly cylindrical rods of the polymer material are embedded in air, whereas in Figure 11 those roles are interchanged: differently shaped pores are embedded into a host consisting of the oxide material (here tantalum pentoxide). Hence, for our purposes, Eq. (A2) can be simplified to:

$$\frac{\varepsilon-\varepsilon_h}{\varepsilon_h+(\varepsilon-\varepsilon_h)L}=p_{guest}\frac{\varepsilon_{guest}-\varepsilon_h}{\varepsilon_h+(\varepsilon_{guest}-\varepsilon_h)L} \tag{A3}$$

When in Figure 11, cylindrical pores are assumed, it holds that L=0.5 for nearly normal incidence, and we obtain:

$$\frac{\varepsilon-\varepsilon_{solid}}{\varepsilon_{solid}+0.5(\varepsilon-\varepsilon_{solid})}=p_{pores}\frac{\varepsilon_{pores}-\varepsilon_{solid}}{\varepsilon_{solid}+0.5(\varepsilon_{pores}-\varepsilon_{solid})} \tag{A4}$$

where ε_{solid} is the dielectric function of the (pore-free) solid oxide material, ε_{pore}=1 for empty pores, and ε_{pore}=1.77 for pores filled with water. This equation is on the basis of the refractive index and shift calculations shown in Figures 12 and 13.

In the system shown in Figure 7, it is the solid fraction that acts as the guest embedded in air, and hence we have:

$$\frac{\varepsilon\text{-}1}{1+0.5(\varepsilon\text{-}1)}=p_{solid}\frac{\varepsilon_{solid}\text{-}1}{1+0.5(\varepsilon_{solid}\text{-}1)} \tag{A5}$$

This equation is identical to Bragg Pippards mixing formula [A5].

In the case that a statistical distribution in the shapes of the inclusions has to be taken into account, the following equation for the effective dielectric function of the mixture can be obtained from Eq. (A3) [A6]:

$$\varepsilon=\varepsilon_h(\lambda)\int_0^1 g(L)\times\frac{1+\dfrac{p_{guest}(1\text{-}L)(\varepsilon_{guest}\text{-}\varepsilon_h)}{\varepsilon_h+(\varepsilon_{guest}\text{-}\varepsilon_h)L}}{1-\dfrac{p_{guest}L(\varepsilon_{guest}\text{-}\varepsilon_h)}{\varepsilon_h+(\varepsilon_{guest}\text{-}\varepsilon_h)L}}\times dL \tag{A6}$$

Here, $g(L)$ represents the normalized distribution in depolarization factors of the individual clusters. Particularly for the characterization tasks mentioned in Section 3.1.3, Eq. (A6) turned out to be rather useful. We emphasize that in Eqs. (A1) to (A6) all ε-values are functions of the frequency.

References

[A1] D. E. Aspnes, J. B. Theeten and F. Hottier, Phys. Rev. B 20, 3292 (1979).

[A2] O. Stenzel, in 'The Physics of Thin Film Optical Spectra', (Springer-Verlag, Berlin Heidelberg, New York, 2005) pp. 45–55.

[A3] L. D. Landau and E. M. Lifschitz, in 'Lehrbuch der theoretischen Physik, Bd. VIII: Elektrodynamik der Kontinua [Textbook of Theoretical Physics, Vol. VIII: Electrodynamics of Continua]', (Akademie-Verlag, Berlin, 1985).

[A4] A. Wokaun, Solid State Phys. 38, 223 (1984).

[A5] H. A. Macleod, in 'Thin-film Optical Filters', (Adam Hilger Ltd., Bristol, 1986).

[A6] M. Bischoff, O. Stenzel, K. Friedrich, S. Wilbrandt, D. Gäbler, et al., Appl. Optics 50, C232 (2011).

References

[1] National Research Council, in 'Harnessing light', (National Academy Press, Washington, DC, 1998) p. 246.

[2] A. Thelen, in 'Design of Optical Interference Coatings', (McGraw-Hill Book Company, New York, 1989) pp. 41–85.

[3] H. A. Macleod, in 'Thin Film Optical Filters', (Institute of Physics Publishing, Bristol/Philadelphia, PA, 2001) pp. 12–85.

[4] W. H. Southwell, Appl. Optics 24, 457 (1985).

[5] S. A. Furman and A. V. Tikhonravov, in 'Basics of Optics of Multilayer Systems', (Edition Frontières, Paris, 1992) pp. 103–151.

[6] A. V. Tikhonravov, Appl. Optics. 32, 5417 (1993).

[7] F. Flory, L. Escoubas and G. Berginc, J. Nanophotonics 5, 052502 (2011).

[8] D. E. Aspnes, J. B. Theeten and F. Hottier, Phys. Rev. B 20, 3292 (1979).

[9] M. Bischoff, O. Stenzel, K. Friedrich, S. Wilbrandt, D. Gäbler, et al., Appl. Optics 50, C232 (2011).

[10] U. Kreibig and M. Vollmer, in 'Optical Properties of Metal Clusters', (Springer Series in Material Science 25, Springer-Verlag, Berlin, Heidelberg, New York, 1995) pp. 13–152.

[11] A. Lebedev, O. Stenzel, M. Quinten, A. Stendal, M. Röder, et al., J. Opt. A Pure Appl. Opt. 1, 573 (1999).

[12] O. Stenzel, S. Wilbrandt, N. Kaiser, M. Vinnichenko, F. Munnik, et al., Thin Solid Films 517, 6058 (2009).

[13] O. Stenzel, J. Phys. D 42, 055312 (2009).

[14] O. Stenzel, S. Wilbrandt, M. Schürmann, N. Kaiser, H. Ehlers, et al., Appl. Optics 50, C69 (2011).

[15] N. K. Sahoo and A. P. Shapiro, Appl. Optics 37, 698 (1998).

[16] B. J. Pond, J. I. DeBar, C. K. Carniglia and T. Raj, Appl. Optics 28, 2800 (1989).

[17] W. J. Gunning, R. L. Hall, F. J. Woodberry, W. H. Southwell and N. S. Gluck, Appl. Optics 28, 2945 (1989).

[18] V. Janicki, D. Gäbler, S. Wilbrandt, R. Leitel, O. Stenzel, et al., Appl. Optics 45, 7851 (2006).

[19] T. V. Amotchkina, V. Janicki, J. Sancho-Parramon, A. V. Tikhonravov, M. K. Trubetskov, et al., Appl. Optics 50, 1453 (2011).

[20] O. Stenzel, S. Wilbrandt, A. Stendal, U. Beckers, K. Voigtsberger, et al., J. Phys. D Appl. Phys. 28, 2154 (1995).

[21] T. V. Amotchkina, M. K. Trubetskov, A. V. Tikhonravov, V. Janicki, J. Sancho-Parramon, et al., Appl. Optics 50, 6189 (2011).

[22] D. G. Mie, Ann. Phys. 25, 377 (1908).

[23] M. Born and E. Wolf, in 'Principles of Optics', (Pergamon Press, Oxford, 1980) pp. 633–665.

[24] L. D. Landau and E. M. Lifschitz, in 'Lehrbuch der theoretischen Physik, Bd. VIII: Elektrodynamik der Kontinua [engl.: Textbook of Theoretical Physics, Vol. VIII: Electrodynamics of Continuous Media]', (Akademie-Verlag, Berlin, 1985) pp. 23–35.

[25] F. Stietz and F. Träger, Physikalische Blätter 55, 57 (1999).

[26] A. Wokaun, Solid State Phys. 38, 223 (1984).

[27] T. Yamaguchi, S. Yoshida and A. Kinbara, Thin Solid Films 21, 173 (1974).

[28] J. M. Gerardy and M. Ausloos, Phys. Rev. B 25, 4204 (1982).

[29] M. Quinten, in 'Optical Properties of Nanoparticle Systems: Mie and Beyond', (Wiley VCH-Verlag & Co. KgaA, Weinheim, 2011) pp. 317–341.

[30] A. N. Lebedev, M. Gartz, U. Kreibig and O. Stenzel, Eur. Phys. J. D 6, 365 (1999).

[31] A. N. Lebedev and O. Stenzel, Eur. Phys. J. D 7, 83 (1999).

[32] P. Heger, O. Stenzel and N. Kaiser, Proc. SPIE 5250, 21 (2004).

[33] V. Janicki, J. Sancho-Parramon and H. Zorc, Appl. Optics 50, C228 (2011).

[34] S. Kachan, O. Stenzel and A. Ponyavina, Appl. Phys. B 84, 281 (2006).

[35] J. A. Schuller, E. S. Barnard, W. Cai, Y. C. Jun, J. S. White, et al., Nat. Mater. 9, 193 (2010).

[36] E. T. Yu and J. van de Lagemaat, MRS Bull. 39, 424 (2011).

[37] S. Hayashi, K. Kozaru and K. Yamamoto, Solid State Commun. 79, 763 (1991).

[38] M. Hiramoto, M. Suezaki and M. Yokoyama, Chem. Lett. 19, 327 (1990).

[39] O. Stenzel, A. Stendal, K. Voigtsberger and C. von Borczyskowski, Sol. Energy Mat. Sol. C. 37, 337 (1995).

[40] O. Stenzel, A. Stendal, M. Röder and C. von Borczyskowski, Pure Appl. Opt. 6, 577 (1997).

[41] M. K. Mogelmose, J. H. Lundsgaard, T. P. Garm, P. Gaiduk and A. L. Nylandsted, Appl. Phys. A Mater. 100, 31 (2010).

[42] J. Jung, T. P. Garm, T. Sondergaard, K. Pedersen, A. L. Nylandstedt, et al., Phys. Rev. B 81, 125413-1 (2010).
[43] S. Wilbrandt, O. Stenzel, M. Bischoff and N. Kaiser, Appl. Optics 50, C5 (2011).
[44] D. Ristau, S. Günster, S. Bosch, A. Duparré, E. Masetti, et al., Appl. Optics 41, 3196 (2002).
[45] K. Iwahori, M. Furuta, Y. Taki, T. Yamamura and A. Tanaka, Appl. Optics 45, 4598 (2006).
[46] M. C. Liu, C. C. Lee, M. Kaneko, K. Nakahira and Y. Takano, Appl. Optics 45, 1368 (2006).
[47] C. C. Jaing, M. H. Shiao, C. C. Lee, C. J. Lu, M. C. Liu, et al., Proc. SPIE 5870 (2005).
[48] G. Atanassov, J. Turlo, J. K. Fu and Y. S. Dai, Thin Solid Films 342, 83 (1999).
[49] M. Bischoff, D. Gäbler, N. Kaiser, A. Chuvilin, U. Kaiser, et al., Appl. Optics 47, C157 (2008).
[50] M. Bischoff, M. Sode, D. Gäbler, H. Bernitzki, C. Zaczek, et al., Proc. SPIE 7101, 71010L (2008).
[51] P. B. Clapham and M.C. Hutley, Nature 244, 281 (1973).
[52] A. Kaless, U. Schulz, P. Munzert and N. Kaiser, Surf. Coat. Tech. 200, 58 (2005).
[53] J. A. Dobrowolski, A. V. Tikhonravov, M. K. Trubetskov, B. T. Sullivan and P. G. Verly, Appl. Optics 35, 644 (1996).
[54] U. Schulz, Opt. Express 17, 8704 (2009).
[55] N. Kaiser and H. K. Pulker, Eds., in 'Optical Interference Coatings', (Springer-Verlag, Berlin, 2003).
[56] H. K. Pulker, S. Schlichtherle, in 'Advances in Optical Thin Films', Eds. By C. Amra, N. Kaiser, H. A. Macleod, Proceedings of SPIE, Vol. 5250 (SPIE, Bellingham, WA, 2004).
[57] F. Jenkner, 'Präparation von TiO_2-, ZrO_2- und HfO_2-Schichten mittels Elektronenstrahlverdampfen', (Bachelorarbeit, Fachhochschule Jena/Fraunhofer IOF, 2011).
[58] O. Stenzel, S. Wilbrandt, S. Yulin, N. Kaiser, M. Held, et al., Opt. Mater. Express 1, 278 (2011).
[59] S. S. Wang and R. Magnusson, Appl. Optics 32, 2606 (1993).
[60] T. V. Amotchkina, J. Sancho-Parramon, V. Janicki, M. K. Trubetskov, H. Zorc, et al., Proc. SPIE 8168, 816809 (2011).
[61] V. Janicki, T. V. Amotchkina, J. Sancho-Parramon, H. Zorc, M. K. Trubetskov, et al., Opt. Express 19, 25521 (2011).
[62] O. Stenzel, Proc. SPIE 5355, 1 (2004).
[63] R. Leitel, P. Heger, O. Stenzel and N. Kaiser, J. Opt. A Pure Appl. Opt. 8, 333 (2006).
[64] O. Stenzel, U. Schulz and N. Kaiser, Proc. SPIE 8104, 810409 (2011).

Olaf Stenzel finished his diploma thesis in laser spectroscopy at the physics department of Moscow State University, Russia, in 1986. He received his PhD from Chemnitz University of Technology, Germany, in 1990 and habilitated there in 1999 in the field of optical properties of heterogeneous optical coatings. From 2001, he has worked at the Optical Coating Department of Fraunhofer Institute for Applied Optics and Precision Engineering IOF in Jena, Germany. He is author of two textbooks in Thin Film Optics and author or co-author of more than one hundred research papers.

Ulrike Schulz received her diploma in physical chemistry in 1986 and her PhD in 1993 from the University of Jena. Since 1997 she heads the group Coating on Plastics in the Optical Thin Film Department of the Fraunhofer Institute for Applied Optics and Precision Engineering in Jena. Her research interests comprise polymer plasma interactions and the design and development of optical coatings on plastics.

Norbert Kaiser received his Diplom Physiker in 1974, his Dr. rer. nat. in 1983 and his Dr. habil in 1999 from the University of Jena, Germany. He is Professor for Physics and Technology of thin films at Technical University Jena. He heads the Optical Thin Film Department and is Vice Director of the Fraunhofer Institute for Applied Optics and Precision Engineering in Jena.